Journal of the Serbian Chemical Society
JSCS-info@shd.org.rs • www.shd.org.rs/JSCS
J. Serb. Chem. Soc. 91 (0) 1–18 (2026)
JSCS–13238
Original scientific paper
Published 12 Feb 2026

Composite materials based on biochar from coffee husk origin and nano zero-valent type Fe/Cu: Potential for treatment of water sources contaminated with As(V)

NGOC TOAN VU[1]*, ANH PHU NGUYEN[2], HONG SON NGUYEN[1], VIET ANH PHAM[1], DINH THAO VU[2] and QUANG MINH LE[3]

[1]*Institute of New Technology, 17, Hoang Sam, Nghia Do, Cau Giay, Hanoi, Vietnam,* [2]*Military Technical Academy, 236, Hoang Quoc Viet, Bac Tu Liem, Hanoi, Vietnam and* [3]*Hanoi–Amsterdam High School for the Gifted, 1, Hoang Minh Giam, Trung Hoa, Cau Giay, Hanoi, Vietnam*

(Received 5 February, revised 6 March, accepted 27 April 2025)

Abstract: In this study, a composite material, Gr–Fe/Cu@BC (CPS), was synthesized using biochar derived from coffee husks and Fe/Cu bimetallic zero-valent nanoparticles for the treatment of water contaminated with As(V). The Fe/Cu bimetallic zero-valent nanoparticles were synthesized *via* a green chemical method employing concentrated *Camellia sinensis* extract as a reducing agent for metal salts. A Box–Behnken experimental design identified optimal conditions for As(V) removal, including a pH range of 5–7, metal/C ratio of approx.-imately 12–13 %, CPS/As mass ratio from 1000 to 1250 and reaction time of around 180 min. The maximum As(V) removal efficiency reached 91.64 % with a maximum adsorption capacity (q_{max}) of 2.86 mg g^{-1}. The adsorption kinetics of As(V) on CPS followed a pseudo-second-order model, with a rate constant (K_2) of 5.96 g mg^{-1} h^{-1}. Furthermore, the structural and surface properties of CPS were characterized using advanced analytical techniques such as SEM, TEM, BET, XRD and EDS, confirming the successful integration of Fe/Cu nanoparticles onto the biochar matrix *via* complexation bonds. These findings highlight the potential of CPS as an environmentally friendly, cost-effective material for the treatment of As(V)-contaminated water and other heavy metal pollutants.

Keywords bimetallic; nanoparticles; water contaminated.

INTRODUCTION

Water contamination by toxic heavy metals, particularly arsenic, has become a significant concern for both environmental safety and human health.[1–3] Arsenic is a toxic element that, upon prolonged exposure, can cause adverse effects on the

* Corresponding author. E-mail: vntoanchem@email.com
https://doi.org/10.2298/JSC250205033V

nervous system, cardiovascular health, dermatological conditions, and liver function.[4,5] Arsenic pollution is now recognized as a global issue, with 21 countries currently facing alarming levels of contamination.[6,7] In particular, regions with naturally elevated geogenic arsenic levels or influenced by anthropogenic activities, such as the Chaco-Pampean plain (Argentina), West Bengal (India), Bangladesh, various parts of Southeast Asia and Limousin (France), have reported serious arsenic contamination in both soil and groundwater sources.[8,9] Inorganic forms of arsenic commonly found in water include As(III) and As(V),[10] with As(V) being highly soluble and mobile in aquatic environments[11] posing substantial challenges to the development of effective remediation technologies. Several conventional methods for arsenic removal have been employed, including ion exchange, coagulation, membrane technologies and adsorption.[1,12–14] Among these, adsorption-based technologies for treating As(V)-contaminated water are widely utilized due to their advantages, such as high removal efficiency, low cost and operational simplicity.[15]

Natural materials have attracted increasing interest as fillers in composite materials due to their widespread availability, cost-effectiveness, straightforward production processes and environmentally friendly nature.[16,17] Coffee husks, a major agricultural by-product of coffee production, represent approximately 30––50 % of the total weight of processed coffee.[18] Vietnam produces approximately 1.47 million tons of coffee annually (2023–2024), generating an estimated 600,000 to 735,000 tons of coffee husks. However, these husks are often underutilized, and their disposal poses environmental challenges.[19] Recent research highlights that composites produced from waste coffee husks exhibit strong potential as adsorbents for removing pollutants from wastewater.[20]

Bimetallic zero-valent nanoparticle systems have emerged as a focal point in environmental remediation research due to their remarkable efficacy in addressing heavy metal contamination.[21–23] Among these, Fe-based bimetallic nanoparticles are particularly noteworthy, offering distinct advantages such as cost-effectiveness, facile synthesis and high catalytic activity. A growing body of evidence underscores that bimetallic zero-valent nanoparticles exhibit superior catalytic performance and enhanced pollutant removal efficiency compared to their monometallic counterparts.[24,25] In recent years, the integration of bimetallic nanoparticles into bio-based matrices has gained prominence as an innovative strategy for nanocomposite synthesis. This approach not only mitigates nanoparticle aggregation but also capitalizes on renewable biomass resources. Shen *et al.*[26] synthesized Fe/Cu bimetallic catalysts supported on biochar derived from paper mill waste, achieving efficient removal of rhodamine B dye. Similarly, Ahmed *et al.*[27] fabricated green Fe/Cu composites using alginate and limestone as substrates for dye degradation in aqueous systems. Additionally, Hoa *et al.*[28] developed Fe/ /Cu@MCM-41 nanomaterials and demonstrated their efficacy in treating reactive

red 195 dye. Collectively, these studies underscore the potential of bimetallic nanocomposites as advanced materials for water treatment applications while highlighting their broader applicability in modern environmental remediation technologies.

This study aims to establish a synthesis protocol for composite materials based on biochar (BC) derived from coffee husks and bimetallic zero-valent nanoparticles Gr–Fe/Cu@BC (CPS). In this process, metal salts react with a concentrated green tea extract (*Camellia sinensis*) as a reducing agent to generate nanoparticles anchored onto the BC matrix. The removal of As(V) from water using CPS was systematically investigated by evaluating key influencing factors, including pH, component ratios and reaction time. Optimal conditions were determined using a response surface methodology approach. The findings of this study provide a foundation for harnessing the potential of CPS in wastewater treatment, particularly for the remediation of heavy metal contaminants.

EXPERIMENTAL

Materials

The chemicals utilized in this study include iron(III) chloride hexahydrate (≥99 %, Xilong, China), copper chloride dihydrate (≥ 99 %, Xilong, China) and concentrated green tea extract (~90 % polyphenols), which was synthesized in our previous study;[29] sodium hydrogen arsenate, $Na_2HAsO_4{\cdot}7H_2O$ (≥99 %, Xilong, China); coffee husks collected from the Đăk Lăk region of the Central Highlands, Vietnam (coordinates 13°06'15.1"N, 108°18'14.9"E), were employed. Other analytical-grade chemicals were used for pH adjustment and desorption processes as needed.

Synthesis of BC

BC was synthesized using a pyrolysis method. Coffee husks (or coffee shells) were thoroughly washed and dried. Approximately 100 g of the coffee husks were placed in a perforated metal container with holes in the lid. The material was then pyrolyzed at 450 °C for 60 min, with the temperature precisely controlled in an SX2-5-12 muffle furnace (China) and allowed to cool naturally. The resulting product was manually ground and sieved through a mesh with a pore size of 0.14 mm to obtain fine powder-form BC (Fig. 1).

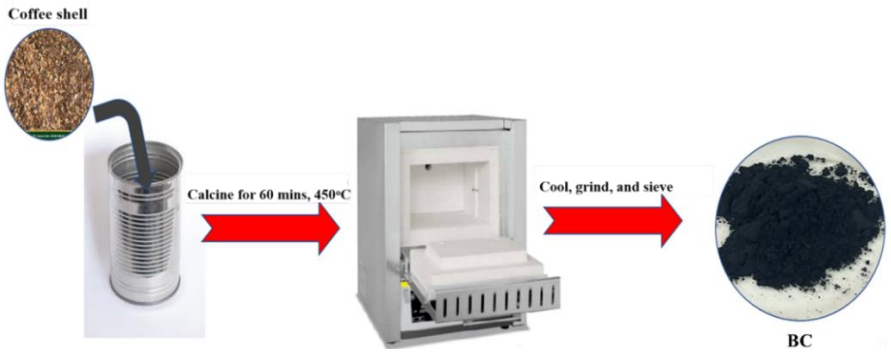

Fig. 1. Synthesis of carbon-based BC material from coffee husk.

Synthesis of CPS

A specified amount of BC was weighed into a 250 mL glass beaker, to which 70 mL of ultrapure water was added. The mixture was stirred at 300 rpm for 15 min at room temperature. A solution of $FeCl_3 \cdot 6H_2O$ and $CuCl_2 \cdot 2H_2O$ was then gradually added to the beaker. Subsequently, a green tea extract solution (green tea powder in water) was slowly introduced into the stirring mixture. The optimal ratio of metal salts and green tea solution was previously reported in our study.[29] The stirring speed was increased to approximately 600 rpm and maintained for 2 h. Afterward, the stirring was stopped and the solution was allowed to stabilize for 5–6 h. The solid product was then filtered, washed three times with 99 % ethanol and transferred to a desiccator for vacuum drying. The final product was left to dry naturally for 8––12 h. The resulting material exhibited a black color and high porosity. The process is schematically represented in Fig. 2.

Fig. 2. Synthesis process of CPS composite.

As(V) removal experiment

A measured quantity of 0.5 g of CPS adsorbent material was placed into a 250 mL Erlenmeyer flask. Subsequently, 100 mL of an As(V) solution with an initial concentration of 5 mg L^{-1} was added to the flask. The mixture was stirred using a magnetic stirrer at 300 rpm under controlled conditions for the designated reaction time. Upon completion of the reaction, the solution was filtered to separate the solid adsorbent and the residual As(V) concentration in the filtrate was analyzed using inductively coupled plasma mass spectrometry (ICP-MS, Agilent 7900, USA). To evaluate the comparative As(V) removal performance, identical experiments were conducted using BC and mono-metallic Gr–12 %Fe/C (containing 12 wt.% Fe) under the same experimental conditions. The removal efficiency of As(V) was calculated using the following formula:

$$R = 100\frac{c_0 - c_t}{c_0} \tag{1}$$

where c_0 (mg L^{-1}) is the initial concentration of As(V), c_t (mg L^{-1}) is the residual concentration of As(V) after treatment.

The post-reaction mixture was filtered to recover the solid material, which was then subjected to desorption by drying at 70 °C for 8 h. This process was repeated over five consecutive cycles to evaluate the reusability of the CPS material.

The setting parameters for the ICP-MS analysis are presented in Table I.

The response surface methodology (RSM) was employed to evaluate the influence of various parameters and optimize the removal efficiency of As(V) from water. A Box–Behnken

experimental design was utilized, involving four independent variables and a fourth-order regression model. The design comprised 30 randomized experimental runs, including five replicates at the center point to ensure statistical reliability. Preliminary exploratory experiments helped define the independent variables and their ranges for the optimization study: pH (X_1, 3––11), reaction time (X_2, 20–180 min), CPS/As mass ratio (X_3, 500–1500), metal/C ratio (X_4, 11––15 %). These variables were coded according to:

$$Y = \beta_0 + \sum_{i-1}^{4} \beta_i X_i + \sum_{i-1}^{4} \beta_{ii} X_i^2 + \sum_{i-1}^{4} \sum_{j-i+1}^{4} \beta_{ij} X_i X_j \quad (2)$$

where Y is the predicted response, X_i and X_j are the coded levels of the independent variables, β_0 is a constant, β_i, β_{ii} and β_{ij} are the model coefficients representing linear, quadratic and interaction effects of variables.

TABLE I. Parameters of ICP-MS setting

Parameter	Value
Forward power	1550 W
Plasma gas	15 L min^{-1}
Kinetic energy discrimination (KED)	3 V
Helium collision gas	No gas
Integration time/point	0.2 s
Replicates	3

Based on Design Expert 13 software, an experimental plan was developed based on the parameters listed in Table II.

TABLE II. Scope of experimental planning of 4 factors

Factor	Unit	Signal	Level				
			–2	–1	0	1	2
A: pH	–	X_1	3	5	7	9	11
B: Reaction time	min	X_2	20	60	100	140	180
C: CPS/As	–	X_3	500	750	1000	1250	1500
D: Metal/C	%	X_4	11	12	13	14	15

Characterization of CPS

The CPS material with the highest As(V) removal efficiency was subjected to comprehensive characterization to assess its structural and compositional properties. The surface morphology of the CPS was analyzed using a scanning electron microscope (SEM, Hitachi S-4800, Japan) and high-resolution transmission electron microscopy (HR-TEM, JEM-2100, Japan). The specific surface area and pore size distribution were determined through Brunauer––Emmett–Teller (BET) analysis (TriStar II 3020, UK). Elemental composition was measured using energy-dispersive X-ray spectroscopy (EDX, Shimadzu EDX-8000, Japan). Additionally, X-ray diffraction (XRD, Panalytical, the Netherlands) was employed to examine the crystalline structure and confirm the formation of crystal phases in the CPS material.

RESULTS AND DISCUSSION

Optimization of As(V) removal conditions using CPS

The efficiency of As(V) removal from aqueous solutions was optimized using a Box–Behnken experimental design. The removal efficiencies obtained under various experimental conditions are presented in Table S-I of the Supplementary material to this paper, ranging from 20.12 to 91.64 %. The highest removal efficiency of 91.64 % was achieved under the conditions of pH 5, reaction time of 140 min, CPS/As mass ratio of 1250 and Fe/Cu ratio of 12 %. By applying multiple regression analysis to the experimental data, the relationship between the response variable (removal efficiency) and the independent variables was modeled using the following second-order polynomial:

$$\begin{aligned} Y = &-229.91782 - 6.45998X_1 + 1.56629X_2 + 0.182551X_3 + 23.76856X_4 - \\ &-0.000952X_1X_2 - 0.000510X_1X_3 + 2.38515X_1X_4 - 0.000193X_2X_3 - \\ &-0.054175X_2X_4 + 0.006548X_3X_4 - 2.12070X_1^2 - 0.001970X_2^2 - \\ &-0.000099X_3^2 - 1.65733X_4^2 \end{aligned} \quad (3)$$

Table III presents the results of the analysis of variance (ANOVA) for the quadratic model. The model exhibited an overall F-value = 17.23 and p-value < 0.0001, indicating its statistical significance at a high confidence level. However, the lack of fit test yielded F-value = 12.93 and p-value = 0.0056, suggesting some discrepancies between the model predictions and the observed data. The analysis of individual factors revealed that pH, reaction time and the CPS/As ratio were the most influential variables on the As(V) removal efficiency, with p-values < 0.0001.

TABLE III. Analysis of variance (ANOVA) for the regression equation

Source	Sum of squares	*df*	Mean square	*F*-value	*p*-value
Model	15112.48	14	1079.46	17.23	< 0.0001
X_1-pH	4124.36	1	4124.36	65.84	< 0.0001
X_2-Time	2762.84	1	2762.84	44.11	< 0.0001
X_3-VL/As	3889.84	1	3889.84	62.10	< 0.0001
X_4-%Fe/Cu	53.67	1	53.67	0.8569	0.3693
X_1X_2	0.0928	1	0.0928	0.0015	0.9698
X_1X_3	1.04	1	1.04	0.0166	0.8992
X_1X_4	364.09	1	364.09	5.81	0.0292
X_2X_3	59.65	1	59.65	0.9523	0.3446
X_2X_4	75.14	1	75.14	1.20	0.2907
X_3X_4	42.88	1	42.88	0.6845	0.4210
Residual	939.60	15	62.64		
Lack of fit	904.62	10	90.46	12.93	0.0056
Pure Eerror	34.98	5	7.00		
Cor total	16052.08	29			

Among these, pH was identified as the most significant factor, exhibiting the highest F-value = 65.84. Conversely, the Metal/C ratio demonstrated a comparatively lower influence, with p-value = 0.3693. The interaction between X_1 and X_4 was found to be statistically significant ($F = 5.81$, $p = 0.0292$), indicating that their combined effect contributed to the efficiency. However, this interaction was less impactful compared to the primary effects of pH and reaction time. Other interactions, including X_1X_2, X_1X_3, X_2X_3, X_2X_4, and X_3X_4 were not statistically significant ($p > 0.05$), suggesting that these factors largely influenced the response independently rather than through synergistic interactions.

Fig. 3a–d presents the 3D response surface plots illustrating the interactive effects of input factors on the removal efficiency of As(V). In Fig. 3a, the interaction between the metal/C ratio and pH indicates that the removal efficiency is highest at a near-neutral pH (5–7). This aligns with the optimal condition to prevent excessive agglomeration of Fe/Cu nanoparticles or reduced material activity in strongly acidic or alkaline environments. Fig. 3b depicts the relationship between CPS/As and pH, showing that increasing CPS concentration under neutral pH conditions significantly enhances removal efficiency due to stronger adsorption capacity. Fig. 3c highlights the combined effect of metal/C and CPS/As, where the removal efficiency peaks at an optimal metal/C ratio of approximately 12–13 %. This is consistent with the uniform surface structure and the enhanced catalytic activity of CPS. The influence of pH and reaction time, as shown in Fig. 3d, indicates that an optimal reaction time of approximately 180 min provides ideal conditions for efficient adsorption and reduction reactions. Fig. 3e shows the correlation between experimental and predicted values of As(V) removal efficiency. The data points are closely aligned along the diagonal, demonstrating the high accuracy of the regression model in predicting outcomes. Finally, the residuals plot (Fig. 3f) reveals that residuals are randomly distributed around zero, with no systematic deviation or trend. This ensures the validity of the statistical model and confirms that the selected input variables are appropriately controlled. In conclusion, the optimization results indicate that CPS performs most effectively under neutral pH (5–7), a metal/C ratio of approximately 12–13 %, CPS/As from 1000 to 1250 and a reaction time of around 180 min. These findings demonstrate the material's potential as a promising solution for As(V) remediation in water.

Adsorption kinetics

The adsorption kinetics model was employed to describe the process of As(V) adsorption onto the surface of CPS. Experimental data were utilized to evaluate the applicability of different kinetic models, including the pseudo-first-order and pseudo-second-order models. These models are mathematically expressed by the following equations:

$$\text{Pseudo-first-order: } \ln(q_e - q_t) = \ln q_e - K_1 t \quad (4)$$

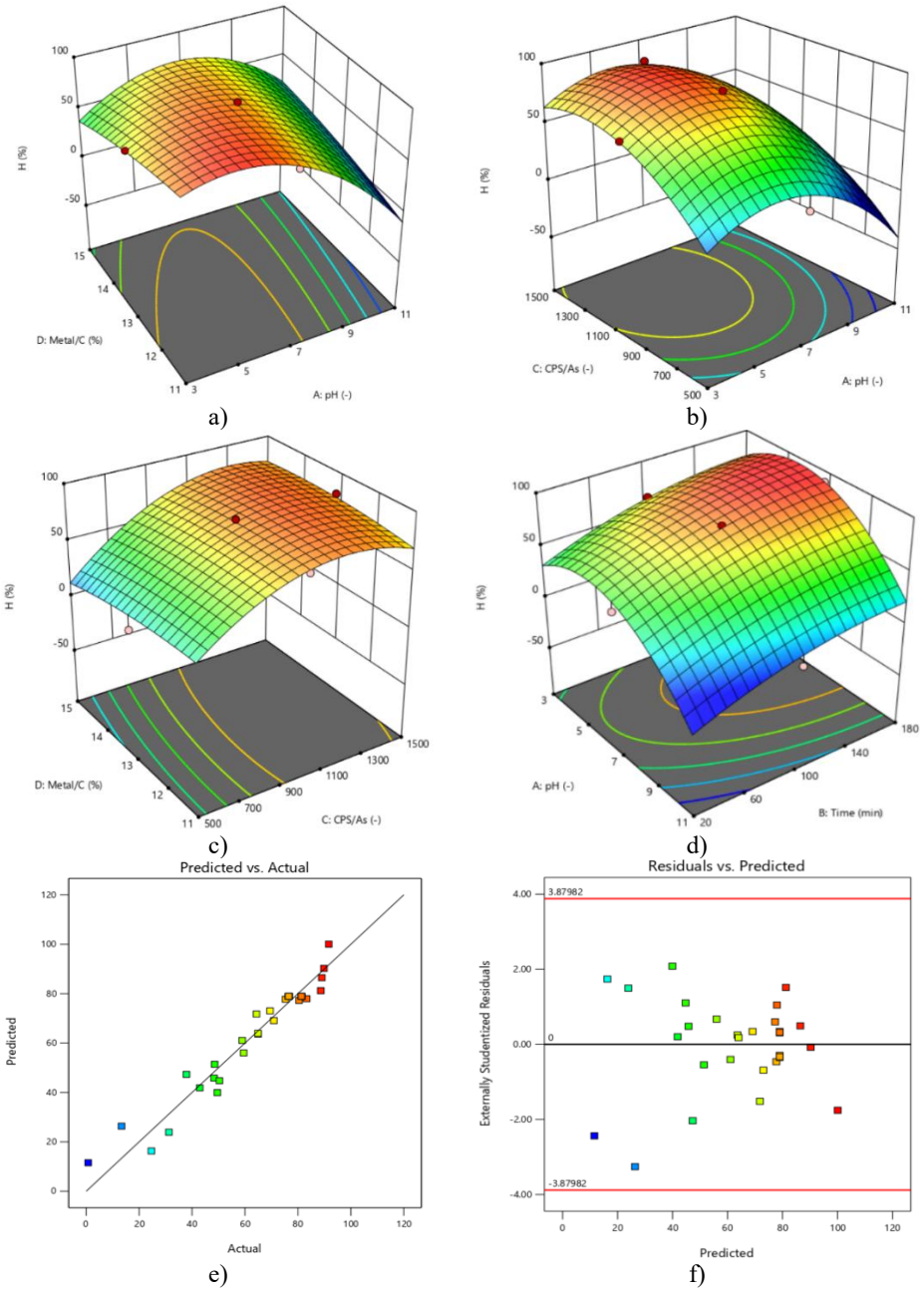

Fig. 3. a–d) RSM model evaluates the influence of factors on As(V) treatment efficiency; e–f) difference between standard data and experimental data.

$$\text{Pseudo-second-order: } \frac{t}{q_t} = \frac{1}{K_2 q_e^2} + \frac{1}{q_e} t \quad (5)$$

where q_e and q_t represent the amount of As(V) adsorbed at equilibrium and at time t, respectively (mg g^{-1}). K_1 and K_2 are the equilibrium rate constants for the pseudo-first-order and pseudo-second-order kinetic models, respectively.

The results depicted in Fig. 4 indicate that the pseudo-second-order kinetic model provides a better fit to the experimental data. This suggests that the adsorption efficiency is influenced by both the concentration of As(V) and the availability of adsorption sites on the material's surface. The kinetic constants and half-adsorption times determined for the studied system are summarized in Table IV.

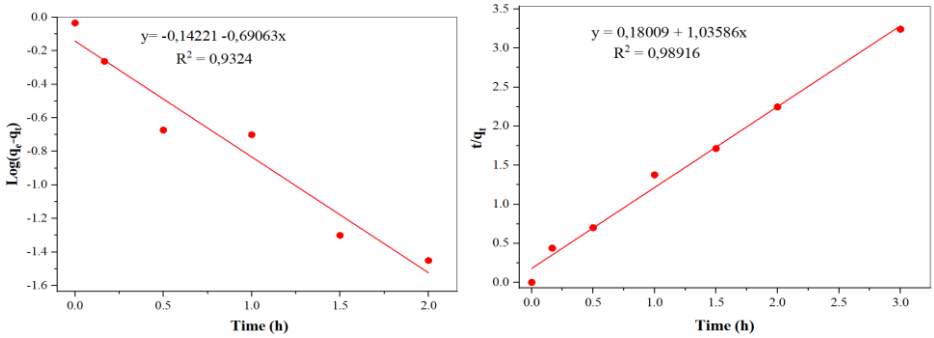

(a) (b)

Fig. 4. a) Pseudo-first-order; b) pseudo-second-order kinetics.

The suitability of the pseudo-second-order model also indicates strong interactions between As(V) ions and the surface of the adsorbent, consistent with a chemisorption mechanism. This suggests that chemical adsorption is the dominant process, overcoming the electrostatic repulsion barrier arising from the electrostatic forces between the composite and As(V) ions.[30] The chemisorption mechanism has been attributed to the formation of surface complexes, where most As(V) ions replace two singly coordinated surface OH groups to form binuclear bridging complexes, specifically Fe–O–AsO(OH)–O–Fe.[31,32]

TABLE IV. Kinetic parameters of As(V) adsorption reaction on CPS

Kinetic model	$K_{1,2}$	$t_{1/2}$	R^2
Pseudo-first-order	0.6906	~1 h	0.9324
Pseudo-second-order	5.96 g mg^{-1} h^{-1}	10.44 min	0.9892

The adsorption isotherms serve to describe the interactions between CPS and the adsorbed species, As(V), at equilibrium. In this study, equilibrium adsorption data for As(V) onto CPS were analyzed using two widely employed two-parameter

isotherm models, Langmuir and Freundlich. These models are mathematically expressed as follows:

$$\text{Langmuir isotherm: } \frac{1}{q_e} = \frac{1}{q_{max} K_L c_e} + \frac{1}{q_{max}} \quad (6)$$

$$\text{Freundlich isotherm: } \ln q_e = \frac{1}{n} \ln c_e + \ln K_F \quad (7)$$

where q_{max} represents the maximum adsorption capacity (mg g^{-1}), K_L is the Langmuir adsorption constant (L mg^{-1}), K_F denotes the Freundlich adsorption constant, and n is the empirical parameter indicative of the adsorption intensity.

The results presented in Fig. 5 demonstrate that the adsorption of As(V) onto CPS follows the Langmuir isotherm model, with a correlation coefficient R^2 = = 0.978, indicating that the predominant adsorption mechanism is monolayer adsorption. The maximum adsorption capacity q_{max} = 2.86 mg g^{-1}, while the Langmuir adsorption constant K_L = 0.82 L mg^{-1}, reflecting the affinity of CPS for As(V). These findings suggest that the adsorption of As(V) occurs on a homogeneous surface of CPS, and the interaction between adsorbed molecules is negligible.

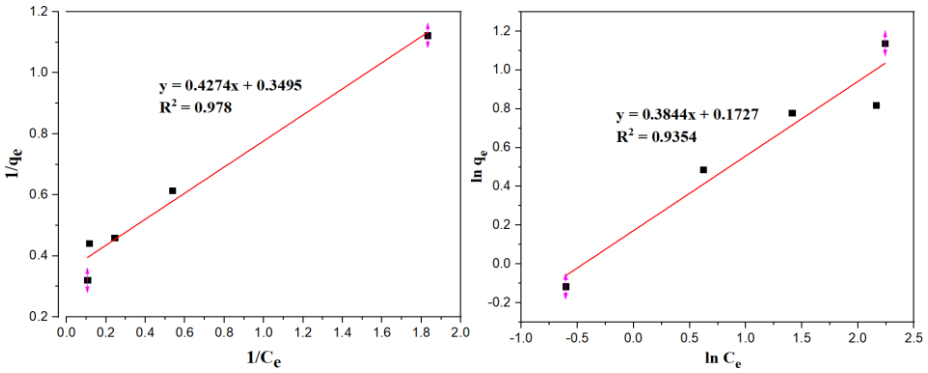

Fig 5. Langmuir and Freundlich isotherm models.

Characterizations of CPS-12%

The BC and composite sample with metal/C = 12 % (CPS-12%) were synthesized and characterized to determine their surface properties. The results, shown in Fig. 6, illustrate the surface morphology of the materials. The BC, after calcination, exists in the form of flakes and relatively fine particles with an average size of approximately 200 nm. The surface of CPS-12% reveals the dispersion of nanoparticles with sizes < 50 nm, adhering to the BC substrate. The nanoparticle distribution on the BC substrate is non-uniform, with some areas showing agglomeration, likely due to the reaction between Fe^{2+}, Cu^{2+} and polyphenolic compounds in the concentrated green tea solution. Additionally, some regions exhibit large gaps between the particles. Analysis of the HR-TEM images of the CPS-12%

sample (Fig. 6c and d) reveals a well-defined crystalline structure with distinct lattice fringes, confirming the successful formation of Fe/Cu nanoparticles. The presence of slightly disordered stacking layers (Fig. 6d) indicates a partially amorphous graphitic carbon support, which is commonly observed in high-surface-area carbon-based materials. The absence of detectable impurity phases suggests that the synthesis method effectively yielded a clean Fe/Cu bimetallic phase uniformly dispersed on the carbon matrix, highlighting its potential for applications in energy storage and catalytic processes. The agglomeration phenomenon in CPS-12% is significantly reduced compared to nanoparticles synthesized via green methods in previous studies by Fang *et al.* [33], and Peili *et al.*[34]

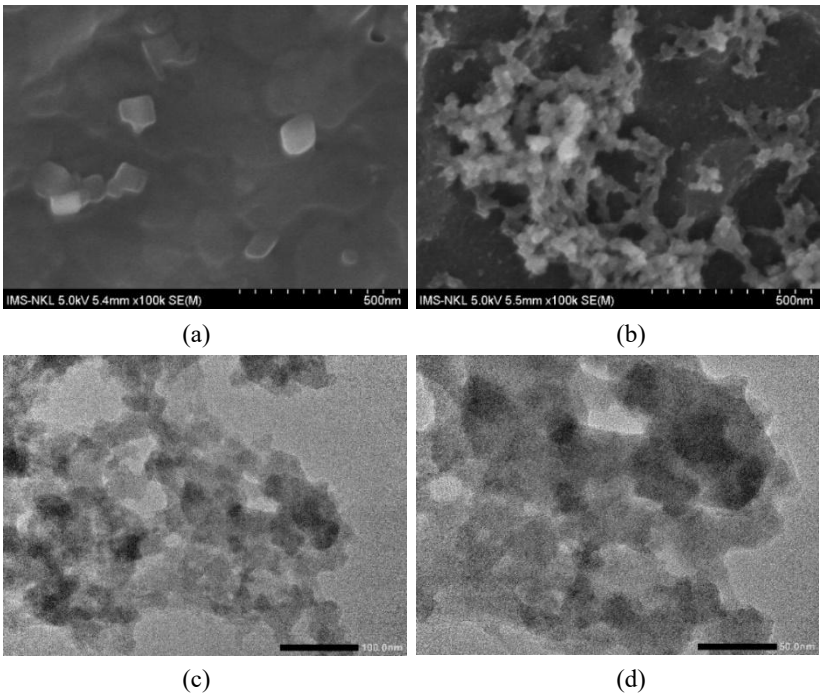

Fig. 6. SEM images of: a) BC from coffee grounds, b) CPS-12%; c,d) HR-TEM images of CPS-12%.

The EDS spectrum results presented in Fig. 7a indicate that the main component of the BC sample is carbon, with a content of 69.88 %, which reflects the carbon-rich nature of the BC. Oxygen constitutes 20.48 %, suggesting the presence of oxidized functional groups on the surface. Elements such as potassium account for 5.08 %, while silicon, phosphorus and sulfur appear at trace levels (< 0.2 %), which may originate from the biomass material or the thermal treatment process.

These characteristics confirm that BC is a stable carbon-based substrate, with surface chemical properties suitable for anchoring metal nanoparticles. The EDS spectrum of the CPS-12 % sample, shown in Fig. 7b, reveals a significant change in composition. The presence of Fe (4.36 %) and Cu (0.37 %) confirms the successful attachment of Fe/Cu nanoparticles onto the BC. Additionally, elements such as P and chlorine (Cl) are detected at low levels, which may be related to impurities or side reactions during the synthesis process.

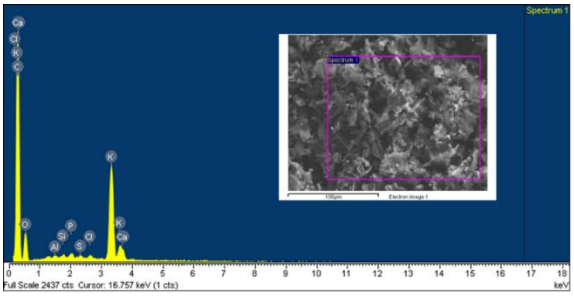

a)

Element	Weight%	Atomic%
C	69.88	79.15
O	20.48	17.41
Al	0.15	0.07
Si	0.18	0.09
P	0.28	0.12
S	0.15	0.06
Cl	0.22	0.08
K	8.08	2.81
Ca	0.58	0.20
Totals	100.00	

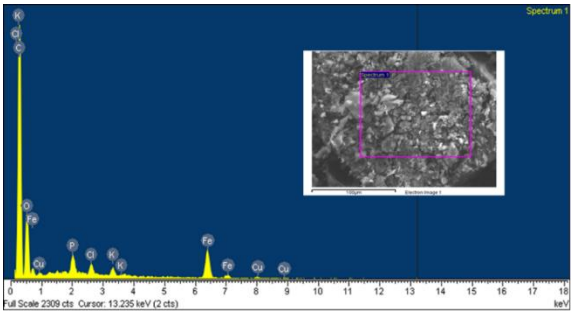

b)

Element	Weight%	Atomic%
C	67.05	75.75
O	26.37	22.37
P	0.87	0.38
Cl	0.53	0.20
K	0.45	0.15
Fe	4.36	1.06
Cu	0.37	0.08
Totals	100.00	

Fig. 7. EDS spectra of: a) BC; b) CPS-12%.

The BET data presented in Fig. 8a–c demonstrate that both BC and CPS-12% exhibit Type IV isotherms, characteristic of mesoporous materials. However, when comparing the two samples, the incorporation of Fe/Cu onto the carbon substrate leads to a slight decrease in specific surface area (from 118.32 to 115.26 $m^2\ g^{-1}$), while the pore volume increases (from 0.1026 to 0.1177 $cm^3\ g^{-1}$). This can be attributed to the deposition of Fe/Cu nanoparticles within the pores, which reduces the average pore size from 50.94 to 44.80 Å, while enhancing pore formation and maintaining the porous structure. Despite these changes, the variation in specific surface area between the two samples is minimal, indicating that the Fe/Cu nanoparticles deposited on the BC surface do not cause significant structural changes. These alterations contribute to an increased surface interaction and enhanced catalytic efficiency of CPS-12%.

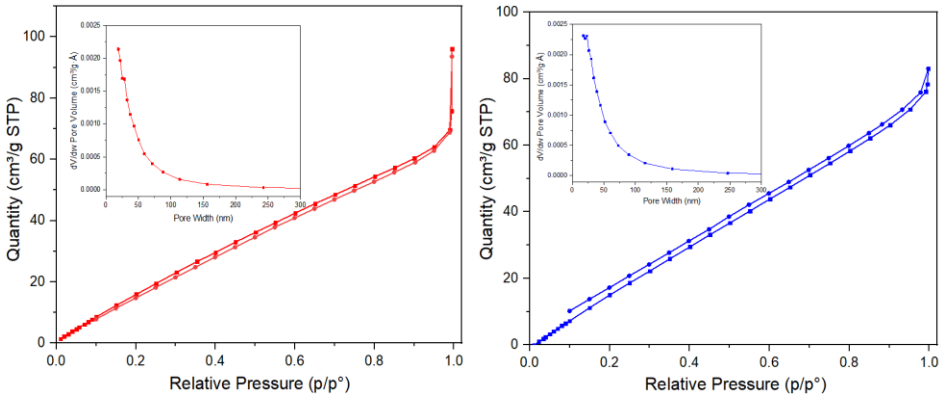

Parameters	Samples	
	BC	CPS-12%
Surface area (S_{BET}), $m^2 g^{-1}$	118,3171	115,2639
Average pore volume, $cm^3 g^{-1}$	0,102591	0,117664
Average pore size, Å	50,940	44,796

c)

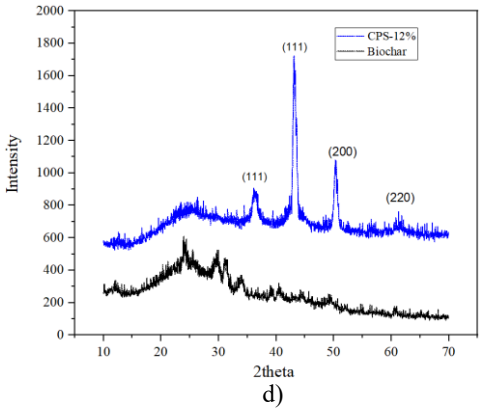

Fig. 8. BET isotherms of: a) BC and b) CPS-12%; c) BET characteristic parameters of BC and CPS-12%; d) XRD of BC and CPS-12%.

As shown in Fig. 8d, the XRD pattern of the initial BC exhibits a broad peak, indicating the amorphous nature of the carbon phase, with characteristic peaks primarily representing the presence of lignocellulose structures.[35,36] The XRD pattern of CPS-12% reveals sharp diffraction peaks. The peak at 2θ 36.1° corresponds to Cu(I) crystals, while the presence of Cu(0) is indicated by peaks at 2θ 43.1 and 50.4°.[37,38] A faint and broad peak at approximately 2θ 44–45° suggests the presence of Fe(0). Additionally, the peak at 2θ 61.2° likely represents the Fe_3C crystals (JCPDS 35-0772),[39] formed due to the interaction between Fe and carbon in the BC substrate.

Comparison of As(V) removal efficiency and reusability of CPS

The results presented in Fig. 9a reflect the As(V) removal efficiency of three samples: BC, Gr–12%Fe@BC and CPS-12%. The As(V) concentration remained almost unchanged when using the pristine BC due to its limited properties, such as

small pore size and low surface functionality. Pristine BC encountered performance limitations when not surface-modified.[40] Surface modification of BC with single-metal Fe nanoparticles, as seen in Gr–12%Fe@BC, led to approximately 60 % As(V) removal at equilibrium. A notable increase in As(V) removal efficiency was observed upon the incorporation of the transition metal Cu to form the Fe/Cu bimetallic system. This enhancement can be attributed to the synergistic effect between Fe and Cu. Pamela *et al.*[41] assume the existence of Cu facilitated electron transfer among Fe, Cu and As, which increased the adsorption rate, capacity and intensity. O'Carrol *et al.*[42] stated that the second metal, in this case Cu, acts as an electronic mediator that catalyzes and increases the removal rates by bimetallic nanoparticles by decreasing the activation energy of the reaction.

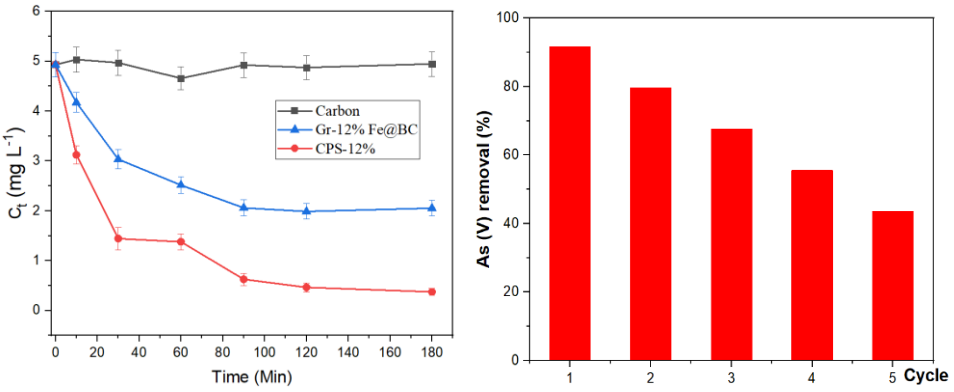

Fig. 9. a) Comparison of As(V) removal efficiency by BC, Gr–12%Fe@BC and CPS-12%; b) As(V) removal efficiency of CPS-12% over 5 reuse cycles.

The decline in As(V) removal efficiency from 91.64 to 45.52 % after five reuse cycles of CPS-12% is depicted in Fig. 9b. Catalytic activity declines primarily due to oxide and hydroxide layers forming on the CPS surface after each treatment cycle, which block Fe–O–As complex formation. Furthermore, partial dissolution of Cu in the CPS under pH conditions of 5–7 ($Cu + 2H^+ \rightarrow Cu^{2+} + + H_2$). The depletion of Cu content reduces the electron transfer rate between Fe and Cu, thereby diminishing the efficiency of the reductive reactions responsible for As(V) removal.[43]

Comparison of As(V) removal efficiency with some other materials

The results in Table V demonstrate a range of removal efficiencies for arsenic and other heavy metals using different materials under varying pH conditions. Most materials achieved moderate efficiencies between 70 and 90 %, often requiring acidic or slightly alkaline environments to perform optimally. In contrast, the CPS material developed in this study exhibited a notably higher As(V) removal

efficiency of 91.64 % at neutral pH, suggesting its superior potential for practical water treatment applications without the need for extensive pH adjustment. This highlights CPS as a promising and efficient alternative among existing materials.

TABLE V. Comparison of heavy metal removal efficiency by materials

No.	Material	Pollutants	Removal efficiency	Ref.
1	Fe_3O_4/AC	As	70 % at pH 8	Joshi *et al.*[44]
2	Bimetallic $Fe_{0.9}Cu_{0.1}$	As(V)	75.223 %	Sepúlveda *et al.*[41]
3	Nano carbon with zirconium	As	70–75 % at pH 2–3	Mahanta *et al.*[45]
4	Carbon/$Fe_3(Mn^{2+})O_4$	As(V)	70–90 % at pH 3	Gallios *et al.*[46]
5	Nano bimetallic Cu–Ni	Cd (II)	70 % at pH 7	Harikumar *et al.*[47]
6	CPS	As (V)	91.64 % at pH 7	This study

CONCLUSION

This study successfully demonstrated the green chemical synthesis of a composite material, CPS, utilizing biochar derived from coffee husks and bimetallic Fe/Cu nanoparticles. The adsorption kinetics were well-fitted to a pseudo-second-order kinetic model, indicating stable and rapid As(V) removal capabilities. Structural analysis confirmed the formation of Fe/Cu nanoparticles with sizes smaller than 50 nm dispersed on the BC matrix. The optimization outcomes further revealed that CPS performs most effectively under near-neutral pH conditions (5–7), with a metal/carbon mass ratio of 0.12–0.13, a CPS/arsenic mass ratio between 1000 and 1250, and a reaction time of approximately 180 min. These findings highlight CPS as a low-cost, environmentally friendly adsorbent with significant potential for applications in the treatment of As(V)-contaminated wastewater. With its sustainability, high efficiency, and reusability over multiple cycles, this research provides valuable insights into the development of advanced adsorbent materials based on renewable resources and green technologies for environmental remediation.

SUPPLEMENTARY MATERIAL

Additional data and information are available electronically at the pages of journal website: https://www.shd-pub.org.rs/index.php/JSCS/article/view/13238, or from the corresponding author on request.

Acknowledgement. The authors acknowledge the facilities and the scientific and technical assistance at the Institute of New Technology/Vietnam.

ИЗВОД

КОМПОЗИТНИ МАТЕРИЈАЛИ НА БАЗИ БИОУГЉА ДОБИЈЕНОГ ОД ЉУСКЕ КАФЕ И НАНО Fe/Cu ЧЕСТИЦА НУЛТОГ ВАЛЕНТНОГ СТАЊА: ПОТЕНЦИЈАЛ ЗА ТРЕТМАН ВОДА КОНТАМИНИРАНИХ АРСЕНОМ(V)

NGOC TOAN VU[1], ANH PHU NGUYEN[2], HONG SON NGUYEN[1], VIET ANH PHAM[1], DINH THAO VU[2] и QUANG MINH LE[3]

[1]Institute of New Technology, 17, Hoang Sam, Nghia Do, Cau Giay, Hanoi, Vietnam, [2]Military Technical Academy, 236, Hoang Quoc Viet, Bac Tu Liem, Hanoi, Vietnam u [3]Hanoi–Amsterdam High School for the Gifted, 1, Hoang Minh Giam, Trung Hoa, Cau Giay, Hanoi, Vietnam

У овом истраживању синтетизован је композитни материјал Gr–Fe/Cu@BC (CPS) употребом биоугља добијеног од љуски кафе и биметалних нултовалентних наночестица Fe/Cu за третман воде контаминиране арсеном(V). Биметалне нултовалентне наночестице Fe/Cu синтетизоване су применом методе "зелене" хемије, користећи концентровани екстракт *Camellia sinensis* као редукционо средство за металне соли. Дизајн експеримента по Box–Behnken моделу идентификовао је оптималне услове за уклањање As(V), укључујући pH у опсегу од 5 до 7, масени однос метал/угљеник од приближно 0,12–0,13, масени однос CPS/As у распону од 1000 до 1250 и време реакције око 180 min. Максимална ефикасност уклањања As(V) достигла је 91,64 %, уз максимални адсорпциони капацитет (q_{max}) од 2,86 mg g^{-1}. Кинетика адсорпције As(V) на CPS пратила је модел псеудо-другог реда, са константом брзине (K_2) од 5,96 g mg^{-1} h^{-1}. Структурне и површинске карактеристике CPS материјала окарактерисане су напредним аналитичким техникама као што су SEM, TEM, BET, XRD и EDS, чиме је потврђена успешна интеграција наночестица Fe/Cu у матрицу биоугља путем координационих веза. Ови резултати указују на потенцијал CPS материјала као еколошки прихватљивог и економичног решења за третман воде контаминиране As(V), као и других загађивача тешким металима.

(Примљено 5. фебруара, ревидирано 6. марта, прихваћено 27. априла 2025)

REFERENCES

1. M. Chiban, G. Carja, G. Lehutu, F. Sinan, *Arab. J. Chem.* **9** (2016) 988 (https://doi.org/10.1016/j.arabjc.2011.10.002)
2. H. Alalwan, A. Alminshid, M. Mohammed, M. Mohammed, M. Shadhar, *Nanomaterials* **8** (2022) 995 (https://doi.org/10.22059/POLL.2022.337436.1329)
3. S. O. Kazantsev, K. V. Suliz, N. G. Rodkevich, A. S. Lozhkomoev, *Materials* **16** (2023) 6057 (https://doi.org/10.3390/ma16176057)
4. K. S. Patel, P. K. Pandey, P. Martín-Ramos, W. T. Corns, S. Varol, P. Bhattacharya, Y. Zhu, *RSC Adv.* **13** (2023) 8803 (10.1039/d3ra00789h)
5. R. N. Ratnaike, *Postgrad. Med. J.* **79** (2003) 391 (https://doi.org/10.1136/pmj.79.933.391)
6. P. Bhattacharyya, Md. M. Alam, in *Contaminants in Agriculture: Sources, Impacts and Management*, M. Naeem, A. A. Ansari, S. Singh Gill, Eds., Springer, Berlin, 2020, pp. 327–337 (https://doi.org/10.1007/978-3-030-41552-5_16)
7. A. Shrivastava, A. Barla, S. Singh, S. Mandraha, S. Bose, *J. Hazard. Mater.* **324** (2017) 526 (https://doi.org/10.1016/j.jhazmat.2016.11.022)
8. V. Antoni, N. Saby, D. Arrouays, C. Jolivet, L. Boulonne, C. Ratie, A. Bispo, T. Eglin, A. Pierart, A. Gay, J.-L. Perrin, I. Joassard, 2019, available at https://www.researchgate.net/publication/331648803_Arsenic_et_mercure_dans_les_sols_francais_pollutions_diffuses_et_ponctuelles

9. R. Singh, S. Singh, P. Parihar, V. P. Singh, S. M. Prasad, *Ecotoxicol. Environ. Saf.* **112** (2015) 247 (https://doi.org/10.1016/j.ecoenv.2014.10.009)
10. X. Ren, H. Feng, M. Zhao, X. Zhou, X. Zhu, X. Ouyang, J. Tang, C. Li, J. Wang, W. Tang, L. Tang, *Int. J. Environ. Res. Pub. Health* **20** (2023) 3829 (https://doi.org/10.3390/ijerph20053829)
11. K. Wrighton-Araneda, D. Cortés-Arriagada, *Chem. Eng. J.* **426** (2021) 131471 (https://doi.org/10.1016/j.cej.2021.131471)
12. H. Saitua, R. Gil, A. P. Padilla, *Desalination* **274** (2011) 1 (https://doi.org/10.1016/j.desal.2011.02.044)
13. L. A. Zemskova, A. V. Voit, D. K. Shlyk, N. N. Barinov, *Russ. J. Appl. Chem.* **89** (2016) 727 (https://doi.org/10.1134/S1070427216050074)
14. G. Zhang, X. Li, S. Wu, P. Gu, *Environ. Earth Sci.* **66** (2012) 1269 (https://doi.org/10.1007/s12665-012-1549-7)
15. Z. Moradi, A. Alihosseini, A. Ghadami, *Res. Mat.* **17** (2023) 100378 (https://doi.org/10.1016/j.rinma.2023.100378)
16. A. Fouly, H. S. Abdo, A. H. Seikh, K. Alluhydan, H. I. Alkhammash, I. A. Alnaser, M. S. Abdo, *Polymers* **13** (2021) 4407 (https://doi.org/10.3390/polym13244407)
17. A. Fouly, I. A. Alnaser, A. K. Assaifan, H. S. Abdo, *Polymers* **14** (2022) 3321 (https://doi.org/10.3390/polym14163321)
18. S. Ponte, *World Develop.* **30** (2002) 1099 (https://doi.org/10.1016/S0305-750X(02)00032-3)
19. P. Murthy, M. Naidu, *Res. Conser. Recyc.* **66** (2012) 45 (https://doi.org/10.1016/j.resconrec.2012.06.005)
20. L.-L. Kang, Y.-N. Zeng, Y.-T. Wang, J.-G. Li, F.-P. Wang, Y.-J. Wang, Q. Yu, X.-M. Wang, R. Ji, D. Gao, Z. Fang, *J. Water Proc. Eng.* **49** (2022) 103178 (https://doi.org/10.1016/j.jwpe.2022.103178)
21. W. S. Abo El-Yazeed, Y. G. Abou El-eash, L. A. Elatwy, A. I. Ahmed, *RSC Adv.* **10** (2020) 9693 (https://doi.org/10.1039/C9RA10300G)
22. S. Cheng, W. Meng, B. Xing, C. Shi, Q. Wang, D. Xia, Y. Nie, G. Yi, C. Zhang, H. Xia, *J. Clean. Prod.* **403** (2023) 136821 (https://doi.org/10.1016/j.jclepro.2023.136821)
23. M. Ajmal, M. Siddiq, N. Aktas, N. Sahiner, *RSC Adv.* **5** (2015) 43873 (https://doi.org/10.1039/C5RA05785J)
24. S. Zhou, Y. Li, J. Chen, Z. Liu, Z. Wang, P. Na, *RSC Adv.* **4** (2014) 50699 (https://doi.org/10.1039/C4RA08754B)
25. A. Behera, B. Mittu, S. Padhi, N. Patra, J. Singh, in *Multifunctional Hybrid Nanomaterials for Sustainable Agri-Food and Ecosystems*, K. A. Abd-Elsalam, Ed., Elsevier Inc., Amsterdam, 2020, pp. 639-–682 (https://doi.org/10.1016/B978-0-12-821354-4.00025-X)
26. Y. Shen, Y. Xiao, H. Zhang, H. Fan, Y. Li, Z. Yan, WH. Zhang, *Chem. Eng. J.* **477** (2023) 146823 (https://doi.org/10.1016/j.cej.2023.146823)
27. I. A. Ahmed, H. S. Hussein, Z. A. Alothman, A. G. Alanazi, N. S. Alsaiari, A. Khalid, *Polymers* **15** (2023) 1221 (https://doi.org/10.3390/polym15051221)
28. T. T. Hoa, L. V. Dung, L. H. Ha, N. B. Manh, *Vietnam J. Cat. Ads.* **9** (2020) 28 (https://doi.org/10.51316/jca.2020.025)
29. N. H. Son, V. H. Nguyen, T. T. H. Nguyen, N. T. Vu, N. H. Le, *Nano Express* **5** (2024) 025026 (https://doi.org/10.1088/2632-959X/ad5221)
30. Y. Lin, X. Jin, N. I. Khan, G. Owens, Z. Chen, *J. Environ. Manage.* **301** (2022) 113838 (https://doi.org/10.1016/j.jenvman.2021.113838)

31. Z. Wu, X. Su, Z. Lin, G. Owens, Z. Chen, *J. Hazard. Mat.* **379** (2019) 120811 (https://doi.org/10.1016/j.jhazmat.2019.120811)
32. J. Zhou, X. Zhou, K. Yang, Z. Cao, Z. Wang, C. Zhou, S. A. Baig, X. Xu, *J. Hazard. Mat.* **384** (2020) 121229 (https://doi.org/10.1016/j.jhazmat.2019.121229)
33. F. Zhu, S. Ma, T. Liu, X. Deng, *J. Clean. Prod.* **174** (2017) 184 (https://doi.org/10.1016/j.jclepro.2017.10.302)
34. P. Ma, Q. Liu, P. Liu, H. Li, X. Han, L. Liu, W. Zou, *J. Disp. Sci. Technol.* **42** (2021) 1350 (https://doi.org/10.1080/01932691.2020.1764367)
35. T. H. Tran, N. T. Vu, P. H. Thien, N. D. Thanh, P. D. Tuan, *Vietnam J. Sci. Tech.* **55** (2017) 516 (https://doi.org/10.15625/2525-2518/55/4/9016)
36. T. S. Andrade, J. Vakros, D. Mantzavinos, P. Lianos, *Chem. Eng. J. Adv.* **4** (2020) 100061 (https://doi.org/10.1016/j.ceja.2020.100061)
37. Z. Xiong, B Lai, P. Yang, *IOP Conf. Ser.: Earth Environ. Sci.* **167** (2018) 012007 (https://doi.org/10.1088/1755-1315/167/1/012007)
38. S.-S. Zhang, N. Yang, S.-Q. Ni, V. Natarajan, H. A. Ahmad, S. Xu, X. Fang, J. Zhan, *RSC Adv.* **8** (2018) 26469 (https://doi.org/10.1039/C8RA04426K)
39. Y. Chen, X.-F. Zhang, A.-J. Wang, Q.-L. Zhang, H. Huang, J.-J. Feng, *Microchim. Acta* **186** (2019) 660 (https://doi.org/10.1007/s00604-019-3769-y)
40. G. Murtaza, Z. Ahmed, D.-Q. Dai, R. Iqbal, S. Bawazeer, M. Usman, M. Rizwan, J. Iqbal, M. I. Akram, A. S. Althubiani, A. Tariq, I. Ali, *Fron. Environ. Sci.* **10** (2022) 1035865 (https://doi.org/10.3389/fenvs.2022.1035865)
41. P. Sepúlveda, M. A. Rubio, S. E. Baltazar, J. Rojas-Nunez, J. L. Sánchez Llamazares, A. G. Garcia, N. Arancibia-Miranda, *J. Coll. Interf. Sci.* **524** (2018) 177 (https://doi.org/10.1016/j.jcis.2018.03.113)
42. D. O'Carroll, B. Sleep, M. Krol, H. Boparai, C. Kocur, *Adv. Water Res.* **51** (2013) 104 (https://doi.org/10.1016/j.advwatres.2012.02.005)
43. C. Settimi, D. Zingaretti, S. Sanna, I. Verginelli, I. Luisetto, A. Tebano, R. Baciocchi, *Sustainability* **14** (2022) 7760 (https://doi.org/10.3390/su14137760)
44. S. Joshi, M. Sharma, A. Kumari, S. Shrestha, B. Shrestha, *Appl. Sci.* **9** (2019) 3732 (https://doi.org/10.3390/app9183732)
45. N. Mahanta, J. P. Chen, *J. Mat. Chem., A* **1** (2013) 8636 (https://doi.org/10.1039/C3TA10858A)
46. G. P. Gallios, A. K. Tolkou, I. A. Katsoyiannis, K. Stefusova, M. Vaclavikova, E. A. Deliyanni, *Sustainability* **9** (2017) 1684 (https://doi.org/10.3390/su9101684)
47. P. S. Harikumar, T.K. Hridya, *Int. J. Environ. Anal. Chem.***101** (2021) 869 (https://doi.org/10.1080/03067319.2019.1673383).